






All-optical ultrafast spin rotation for relativistic charged particle beams

Wen-Qing Wei ¹, Feng Wan,^{1,*} Yousef I. Salamin ², Jie-Ru Ren,¹ Karen Z. Hatsagortsyan,³
Christoph H. Keitel ³, Jian-Xing Li ^{1,†} and Yong-Tao Zhao ^{1,‡}

¹Ministry of Education Key Laboratory for Nonequilibrium Synthesis and Modulation of Condensed Matter,
Shaanxi Province Key Laboratory of Quantum Information and Quantum Optoelectronic Devices,
School of Physics, Xi'an Jiaotong University, Xi'an 710049, China

²Department of Physics, American University of Sharjah, P.O. Box 26666 Sharjah, United Arab Emirates

³Max-Planck-Institut für Kernphysik, Saupfercheckweg 1, 69117 Heidelberg, Germany



(Received 12 January 2022; revised 28 November 2022; accepted 24 February 2023; published 17 April 2023)

An all-optical method of ultrafast spin rotation is put forward to precisely manipulate the polarization of relativistic charged particle beams of leptons or ions. Laser-driven dense ultrashort beams are manipulated via single-shot interaction with a copropagating temporally asymmetric laser pulse of moderate intensity. Using semiclassical numerical simulations, we show that the initial polarization of a lepton (proton) beam can be rotated to any desired orientation by a flexible control over the phase retardation between the spin precession and the momentum oscillation in a temporally asymmetrical (e.g., half-cycle terahertz or frequency-chirped) laser field. In particular, spin ultrafast rotation from the common transverse to the more valuable longitudinal polarization is feasible in a picosecond scale or less. Moreover, the beam quality, in terms of energy and angular divergence, is improved in the rotation process. This method has potential applications in various areas demanding ultrafast spin manipulation, like laser-plasma, laser-nuclear, and high-energy physics.

DOI: [10.1103/PhysRevResearch.5.023030](https://doi.org/10.1103/PhysRevResearch.5.023030)

I. INTRODUCTION

Relativistic beams of spin-polarized charged particles, such as leptons and protons, play a crucial role in exploring fundamental structures [1–3] and interactions [4–7], with the advantage of an increased number of measurable observables and unprecedented test precision [8,9]. They can provide direct access to study new physics beyond the standard model [10], characterize the quantum numbers and chiral couplings of new particles [8,11], investigate spin-dependent nuclear interactions [12–14], and increase the cross section and control the angular distribution of the reaction products in nuclear fusion reactions [15,16]. In the famous proton-spin puzzle [17,18], energetic polarized proton beams are applied to precisely measure the internal spin-flavor structure of the quarks and the gluon spin distribution of the target proton in proton-proton collisions [19–23]. In these experiments, the longitudinal spin polarization is generally sensitive to the helicity distributions of the quarks and gluons [19,23], while the transverse one is sensitive to the transversity distributions of quarks and parton orbital angular momenta

[3,20]. The production of longitudinally spin-polarized (LSP) and transversely spin-polarized (TSP) particle beams with a high degree of polarization ($\gtrsim 70\%$ [3,8]) is, therefore, quite desirable.

In general, the production of a relativistic polarized proton beam is accomplished in two steps. First, a low-energy beam is produced from an optically pumped polarized H^- ion source [24] or a polarized atomic beam source [25], and then injected into a high-energy accelerator, where it is commonly rotated to the TSP state in order to suppress the depolarization effect. A relativistic TSP electron beam, by comparison, can be obtained from a low-energy one produced by photoemission from a GaAs-based cathode [26] and then accelerated by conventional means, or directly employing the Sokolov-Ternov effect in a storage ring [27]. Relativistic LSP proton and electron beams are obtained via spin-polarization manipulation in conventional spin rotators [28,29] and Siberian snakes [30,31] (the latter are employed to avoid the polarization loss due to imperfections and intrinsic depolarizing spin resonances [30,32]), both of which consist of a sequence of vertical and horizontal arc dipoles and superconducting solenoids (or specially arranged magnets). The conventional spin rotators manipulate the polarization adiabatically, and the manipulation precision is sensitive to the beam energy spread and the perturbing fields around the particle trajectories. They generally take tens of minutes or even hours to switch between TSP and LSP states and typically run a few times per day in order to cancel the remaining potentially undesirable systematic effects [3,29].

Rapid advances in ultraintense ultrashort laser technique, with peak intensities reaching the scale of 10^{23} W/cm², pulse

*wanfeng@xjtu.edu.cn

†jianxing@xjtu.edu.cn

‡zhaoyongtao@xjtu.edu.cn

durations of tens of femtoseconds, and energy fluctuations of about 1% [33–35], offer new avenues for polarized beam generation. Relatively low-cost and efficient laser-driven plasma accelerators with a gradient exceeding 0.1 TeV/m are capable of providing dense tens-of-MeV proton [36–38] and multi-GeV electron beams [39] with a bunch size of several micrometers, divergence of approximately milliradians, and moderate charge of pC-nC. In all-optical setups, leptons can be transversely polarized in standing-wave [40–42], elliptically polarized [43,44], or bichromatic laser pulses [45–48] due to the quantum radiative spin-flip effect, since the transverse laser field dominates the spin-polarization process; while the more useful LSP lepton beams can only be produced indirectly via the helicity transfer from circularly polarized γ photons in linear [49] or nonlinear Breit-Wheeler pair production processes [50,51]. The latter is generally reproduced via Compton scattering [52] or bremsstrahlung [53]. High-energy polarized electron [54–56] and proton beams [57–59] can also be produced through laser-driven wakefield acceleration of prepolarized low-energy ones, generated via a photodissociated hydrogen halide gas target [60–62]. Unfortunately, ultrafast spin manipulation of these beams, in particular, spin rotation from the TSP to the LSP state, is still a great challenge.

In this paper, an all-optical ultrafast spin rotation method is put forward to precisely manipulate the polarization of relativistic (laser-driven) ultrashort particle beams through interaction with a copropagating moderate temporally asymmetrical (e.g., half-cycle terahertz or frequency-chirped) laser pulse (see Fig. 1). The focus will be on the transformation of the TSP state of a lepton or proton beam into the LSP state (or any desired polarization state). This will be achieved with high manipulation precision better than 3%, while moderately improving beam qualities in terms of the energy and angular divergence (see Figs. 2 and 4). We find that in a strong laser field the rotation of a particle’s spin is determined by the phase retardation between its spin precession and momentum oscillation, which can be flexibly controllable for temporally asymmetrical laser fields (see Figs. 3 and 5). This method is demonstrated to be robust with respect to the parameters of the laser and particle beams (see Figs. 6 and 7), is realizable with currently achievable laser technique, and thus has significant applications in broad areas involving ultrafast spin manipulation.

II. METHODS OF THEORY AND NUMERICAL SIMULATION

In our simulations the particle’s spin and momentum dynamics will be treated semiclassically. For an electron the quantum radiation effects are characterized by the invariant parameter $\chi \equiv |e|\hbar\sqrt{(F_{\mu\nu}p^\nu)^2}/m_e^3c^4 \approx a_0\gamma(\hbar\omega_0/m_e c^2)(1 - |\boldsymbol{\beta}| \cos\theta)$ [63,64], where \hbar is the Planck constant and c the speed of light; p^ν , $\boldsymbol{\beta}$, γ , e , and m_e are the four-momentum, velocity normalized by c , Lorentz factor, charge, and mass of the electron, respectively. Also, $F_{\mu\nu}$, ω_0 , $a_0 \equiv |e|E_0/(m_e\omega_0 c)$, and E_0 are the field tensor, frequency, invariant intensity parameter, and amplitude of the laser pulse, respectively. For the employed parameters, we have $\chi_e \sim 10^{-7}$ for electrons, and $\chi_p \sim 10^{-8}$ for protons. With $\chi \ll 1$, the Compton

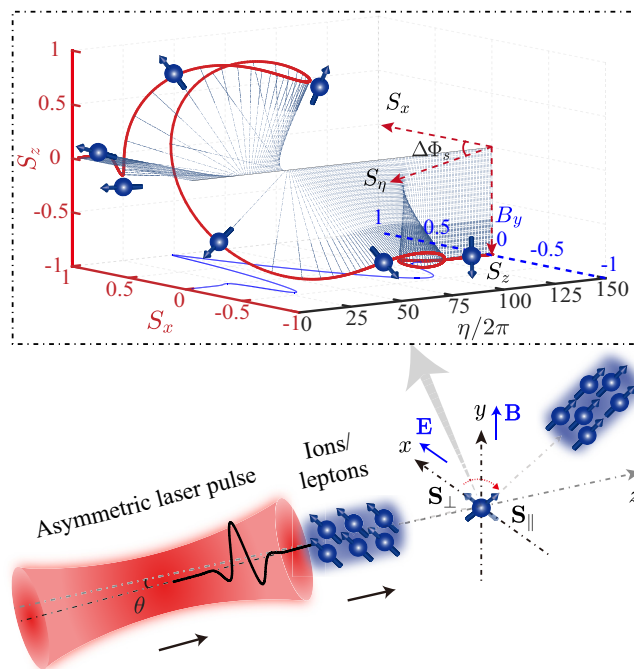


FIG. 1. Interaction scenario. The TSP particle beam (“ S_{\perp} ,” along the $+x$ direction and perpendicular to its initial momentum direction) is rotated to the LSP state (“ S_{\parallel} ,” parallel to its final momentum direction). \mathbf{E} and \mathbf{B} indicate the electric and magnetic components of the laser field, respectively. Inset: particle spin evolution. θ is the laser incidence angle with respect to the normal direction of the particle-beam target, $\Delta\Phi_s$ is the spin rotation angle, and η is the laser phase.

scattering induced quantum radiation reaction effects on the particle’s dynamics and radiative spin polarization (Sokolov-Ternov effect) are negligible [54–59,65–69]. Furthermore, the Stern-Gerlach force and the space-charge force are much smaller than the Lorentz force in our simulations and can be neglected [70,71]. Thus the particle motion can be adequately described by Newton-Lorentz equations, and the spin precession is governed by Thomas-Bargmann-Michel-Telegdi equation [72–74]:

$$d\mathbf{S}/d(\omega_0 t) = \boldsymbol{\Omega}_s \times \mathbf{S}, \tag{1}$$

where

$$\boldsymbol{\Omega}_s = -\frac{q}{m} \left[\left(a + \frac{1}{\gamma} \right) \mathbf{B} - \frac{a\gamma}{\gamma + 1} (\boldsymbol{\beta} \cdot \mathbf{B}) \boldsymbol{\beta} - \left(a + \frac{1}{\gamma + 1} \right) (\boldsymbol{\beta} \times \mathbf{E}) \right]. \tag{2}$$

Dimensionless units are used throughout: q , m , and $\boldsymbol{\Omega}_s$ are the particle charge, mass, and precession frequency normalized by e , m_e , and ω_0 , respectively, \mathbf{E} and \mathbf{B} are normalized by $|e|/(m_e\omega_0 c)$, \mathbf{S} is the particle’s spin vector in its rest frame, and $a = (g - 2)/2$ is the anomalous magnetic moment of the particle with the gyromagnetic factor g [75]. For the electron and proton, $a \approx 1.16 \times 10^{-3}$ and 1.793, respectively.

The scenario of the spin-polarization rotation of a particle beam in a temporally asymmetrical laser pulse is illustrated in Fig. 1. An initially TSP particle beam, with the spin vector $(\hat{S}_x, \hat{S}_y, \hat{S}_z) = (1, 0, 0)$ copropagates with the laser pulse. The pulse is linearly polarized along $+x$ and propagates with $\theta = 5^\circ$ along $+z$. The particles are initially distributed in a cylinder of radius $R = 1.5\lambda_0$ and length $L = 0.5\lambda_0$, with a number density $n_0 \approx 2.26 \times 10^{16} \text{ cm}^{-3}$. The distribution is transversely Gaussian and longitudinally uniform. The initial kinetic energy of the particle beam is $\varepsilon_0 = 1 \text{ MeV}$ with 1% energy spread, and the angular divergence is about 11.8° . Such prepolarized beams can be obtained via photodissociation of the aligned hydrogen halide molecules with circularly polarized ultraviolet light with a density range of 10^{16} – 10^{19} cm^{-3} [60–62].

In our interaction geometry of $\mathbf{E} = \hat{i}E_x$ and $\mathbf{B} = \hat{j}B_y$ with small γ , one gets the spin precession frequency $\boldsymbol{\Omega}_s \simeq -\frac{q}{\gamma m}(\gamma a + 1)\mathbf{B} = -C\mathbf{B}$ and $\Omega_{s,x} \simeq \Omega_{s,z} \approx 0$, with $C = \frac{q}{m}(a + \frac{1}{\gamma})$. Thus one can obtain

$$\begin{aligned}\dot{S}_x &= \Omega_{s,z}S_y - \Omega_{s,y}S_z \simeq -\Omega_{s,y}S_z, \\ \dot{S}_y &= \Omega_{s,x}S_z - \Omega_{s,z}S_x \simeq 0, \\ \dot{S}_z &= \Omega_{s,y}S_x - \Omega_{s,x}S_y \simeq \Omega_{s,y}S_x,\end{aligned}\quad (3)$$

which further induce

$$\dot{S}_z^2 + \Omega_{s,y}^2 S_z^2 - \Omega_{s,y}^2 = 0. \quad (4)$$

Due to $S_z \in [-1, 1]$, we can take a natural choice of solution of $S_z(t) = \sin[\Delta\Phi_s(t) + \theta_0]$ and consequently get

$$\cos^2[\Delta\Phi_s(t) + \theta_0]\Delta\dot{\Phi}_s^2(t) = \Omega_{s,y}^2 \cos^2[\Delta\Phi_s(t) + \theta_0]. \quad (5)$$

Hence the spin rotation angle is

$$\Delta\Phi_s(t) \simeq \int_0^\tau |\Omega_{s,y}| dt, \quad (6)$$

where τ is the particle precession time in the field, and θ_0 the initial polarization angle (for a TSP particle beam $\theta_0 = 0$).

Firstly, we employ a loosely focused half-cycle terahertz laser pulse with the field modeled as $B_y \simeq E_x = a_0 \cos(\varphi_0 + \eta) \exp[-(\eta - 4\tau_0/T_0)^2/(\tau_0/T_0)^2]$, corresponding to the measured terahertz pulse shape in experiments [76–78] (Fig. 1). Here a_0 is the laser normalized amplitude, φ_0 the carrier-envelope phase (CEP), τ_0 the pulse duration with period T_0 , $\eta = \omega_0(t - z/c)$, and ω_0 the initial frequency at $z = 0$. Ignoring the Gaussian pulse envelope, we get

$$\Delta\Phi_{s(\text{half-cycle-THz})} \approx a_0 C \sin(\varphi_0 + \eta) + C_0, \quad (7)$$

where C_0 is an integration constant. $\Delta\Phi_s$ depends sensitively on the time-integrated $\boldsymbol{\Omega}_s$ (subsequently on \mathbf{B}) and further on a_0 , τ_0 , g factor, and particle charge-to-mass ratio. In the simulations, we set $a_0 = 2.5$ (the peak power $\sim 1 \text{ TW}$) with wavelength $\lambda = 300 \mu\text{m}$, $\tau_0 = 0.5T_0$, $\varphi_0 = 0$, and focal radius $w_0 = 1 \text{ mm}$. Such subcycle terahertz pulses can be generated in experiments mostly via coherent transition radiation and sheath radiation from relativistic laser-foil interactions [76–78].

In addition, a focused strongly linearly frequency-chirped Gaussian laser pulse could also be another candidate as a drive field with broken temporal symmetry [79,80]. The pulse

instantaneous frequency is $\omega(\eta) = \omega_0(1 + b\eta)$, where b is the dimensionless chirp parameter. For convenience of calculations, the spin rotation angle can be analytically estimated by using a plane wave with uniform spatial distribution as $B_y \simeq a_0 \cos(\varphi_0 + \eta + b\eta^2)$, then

$$\begin{aligned}\Delta\Phi_{s(\text{chirp})} &\simeq \int_0^{\eta'} a_0 C \cos(\eta + b\eta^2) d\eta \\ &= a_0 C \int_0^{\zeta'} \frac{\cos \zeta}{\sqrt{4b\zeta + 1}} d\zeta,\end{aligned}\quad (8)$$

where $\zeta = \eta + b\eta^2$, $\zeta' = \eta' + b\eta'^2$. Thus,

$$\begin{aligned}\Delta\Phi_{s(\text{chirp})} &\simeq a_0 C \left\{ \sqrt{\frac{\pi}{2b}} \left[\cos\left(\frac{1}{4b}\right) \text{Fresnel C}\left(\frac{1 + 2b\eta'}{\sqrt{2\pi b}}\right) \right] \right. \\ &\quad \left. + \sin\left(\frac{1}{4b}\right) \text{Fresnel S}\left(\frac{1 + 2b\eta'}{\sqrt{2\pi b}}\right) \right\} + C_0,\end{aligned}\quad (9)$$

and, at the phase η' , $S_z(\eta') \simeq \sin[\Delta\Phi_s(\eta') + \theta_0]$. It shows that $\Delta\Phi_s$ and then the particles final spin state are closely related to the chirp parameter b . In the sample cases of the interaction with proton (electron) beam, $a_0 = 50$ (0.2), $\lambda_0 = 1 \mu\text{m}$, $\tau_0 = 30T_0$ ($10T_0$), $w_0 = 5 \mu\text{m}$, and $b = -0.00539$ (-0.0167).

Similarly, the particle motion is described by the Newton-Lorentz equation of $d\mathbf{p}/dt = q(\mathbf{E} + \boldsymbol{\beta} \times \mathbf{B})$. Since $d\gamma/dt \ll 1$ in our simulations, one can get $d\boldsymbol{\beta}/dt \approx (\mathbf{E} + \boldsymbol{\beta} \times \mathbf{B})q/\gamma m$. We define the particle momentum direction $\hat{\mathbf{n}} \equiv \boldsymbol{\beta}/\beta$, then

$$\frac{d\hat{\mathbf{n}}}{dt} = \frac{\dot{\boldsymbol{\beta}}}{\beta} - \frac{\boldsymbol{\beta}}{\beta^3}(\boldsymbol{\beta} \cdot \dot{\boldsymbol{\beta}}) = \boldsymbol{\Omega}_p \times \hat{\mathbf{n}}. \quad (10)$$

We further get

$$\begin{aligned}\frac{d\hat{\mathbf{n}}}{dt} &= \frac{q}{\gamma m \beta} [\boldsymbol{\beta} \times \mathbf{B} + \mathbf{E} - \boldsymbol{\beta}(\boldsymbol{\beta} \cdot \mathbf{E})] \\ &\quad - \frac{q\boldsymbol{\beta}}{\gamma m \beta^3} [\boldsymbol{\beta} \cdot (\boldsymbol{\beta} \times \mathbf{B}) + \boldsymbol{\beta} \cdot \mathbf{E} - \beta^2(\boldsymbol{\beta} \cdot \mathbf{E})] \\ &= \frac{q}{\gamma m} \left[-\mathbf{B} \times \hat{\mathbf{n}} + \frac{\mathbf{E}}{\beta} - \beta \hat{\mathbf{n}}(\hat{\mathbf{n}} \cdot \mathbf{E}) \right. \\ &\quad \left. - \frac{\hat{\mathbf{n}}}{\beta}(\hat{\mathbf{n}} \cdot \mathbf{E}) + \beta \hat{\mathbf{n}}(\hat{\mathbf{n}} \cdot \mathbf{E}) \right] \\ &= \frac{q}{\gamma m} \left[-\mathbf{B} + \frac{1}{\beta}(\hat{\mathbf{n}} \times \mathbf{E}) \right] \times \hat{\mathbf{n}}.\end{aligned}\quad (11)$$

Hence,

$$\boldsymbol{\Omega}_p = \frac{q}{\gamma m} \left[\frac{\hat{\mathbf{n}} \times \mathbf{E}}{\beta} - \mathbf{B} \right]. \quad (12)$$

Here, for the giving parameters, $\Omega_{p,x} \simeq \Omega_{p,z} \approx 0$, and $\Delta\Phi_p(t) \simeq \int_0^\tau |\Omega_{p,y}| dt$. Therefore, the spin-polarization direction of the particle beam, i.e., its spin direction ($\Delta\Phi_s$) with respect to its momentum direction ($\Delta\Phi_p$), is determined by the phase retardation $|\Delta\Phi_s - \Delta\Phi_p|$.

III. RESULTS AND DISCUSSION

A. Electron beam in a half-cycle terahertz laser pulse

In this section, we begin by discussing the spin-polarization rotation following the example of an electron

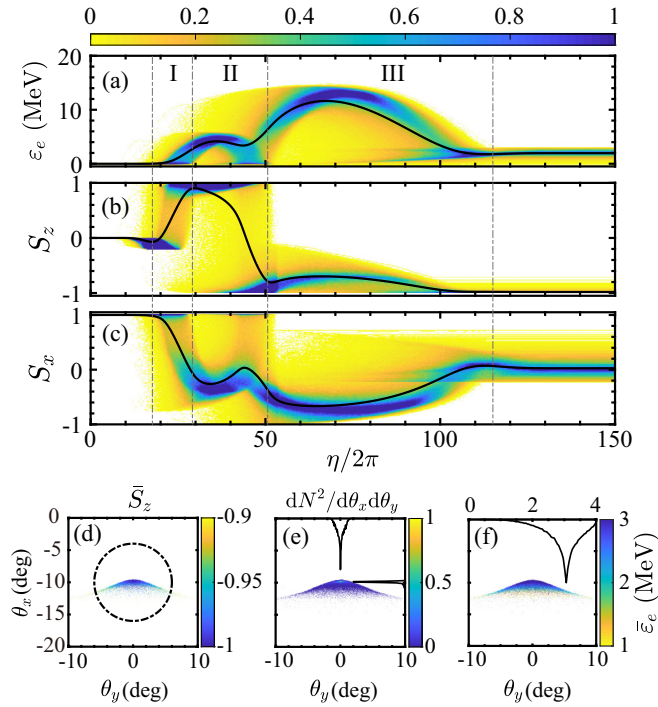


FIG. 2. (a)–(c) Variations of $dN/d\varepsilon_e$, dN/dS_z , and dN/dS_x of the electron beam (color) with respect to η , respectively, and the black curves show the corresponding average values. N is the particle number. Finally angle-resolved distributions of (d) \bar{S}_z , (e) density, and (f) energy $\bar{\varepsilon}_e$ vs the transverse deflection angles $\theta_x = \arctan(p_x/p_z)$ and $\theta_y = \arctan(p_y/p_z)$ for the electron beam, respectively. The black-dashed circle and black-solid curves denote the corresponding beam initial profile size, density lineouts at the center of $\theta_x = -9.84^\circ$, $\theta_y = 0^\circ$, and the final energy spectrum, respectively. Simulation parameters are given in the text.

beam in a half-cycle terahertz laser pulse (see Fig. 2). Consider what happens as the front of the laser pulse catches up and interacts with the electrons [region I in Figs. 2(a)–2(c); $18 \lesssim \eta/2\pi \lesssim 30$]. The electron spins oscillate promptly, with S_z increasing up to 1, while S_x reduces down to zero. Subsequently, S_z drops off significantly and then flips to the opposite direction, whereas S_x continues to oscillate with the rising edge of the laser field from zero to -0.7 [region II; $30 \lesssim \eta/2\pi \lesssim 50$]. Thereafter, the electron spins vary gently within ~ 30 ps and finally their oscillations keep stable with the average spins of $\bar{S}_z \simeq -0.98$ and $\bar{S}_x \simeq 0.03$ during the interaction with the falling edge of the laser field [region III; $\eta/2\pi \gtrsim 50$]. This allows us to rotate the spin polarization of the electron beam from the TSP state (\mathbf{S}_\perp , denoted by S_x in the interaction geometry of Fig. 1, in which $S_y \approx 0$) to the LSP state (\mathbf{S}_\parallel , denoted by S_z) within the scale of picoseconds. The final average polarization is $\sim 98.2\%$ with a bell-shaped angular distribution along θ_y [see Fig. 2(d)], and the electron beam is evidently compressed by the laser field, in particular, in θ_x to less than 2° , which results from the transverse ponderomotive force [$\sim \Delta p_{x,y}/p_z$; see Fig. 2(e)]. Moreover, the electron beam is slightly accelerated with an average energy gain of about 2 MeV due to the phase

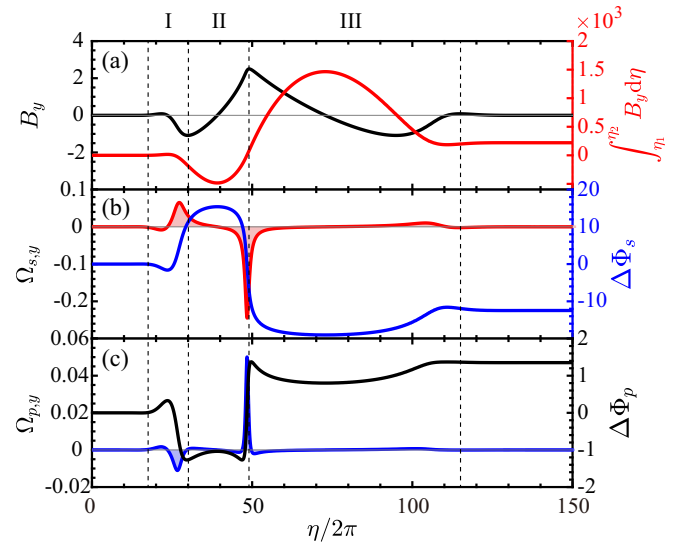


FIG. 3. (a) Evolutions of the normalized magnetic field B_y , sensed by the electron (black) and its local time-integrated profile (red). (b) Spin precession frequency $\Omega_{s,y}$ (red) and $\Delta\Phi_s$ (blue) vs η . (c) Momentum angular frequency $\Omega_{p,y}$ (blue) and $\Delta\Phi_p$ (black) vs η . Other simulation parameters are the same as those in Fig. 2.

synchronization between the laser and electron beam, and its energy spread is $\sim 9.8\%$ [see Fig. 2(f)]. These results may be optimized further by moderately increasing the laser focal radius and intensity, allowing the electrons to experience a quasiuniform laser field and achieve remarkable energy gain.

The details of the spin manipulation mechanism are analyzed in Fig. 3. In the interaction geometry of Fig. 1, $\mathbf{E} = \hat{i}E_x$ and $\mathbf{B} = \hat{j}B_y$. For electrons with low average $\gamma \approx 6.8$ [see Fig. 2(a)], the spin precession frequency $\Omega_{s,x} \simeq \Omega_{s,z} \approx 0$ and maximum $\Omega_{s,y} \approx -0.25$. The corresponding angular frequency of the momentum $\Omega_{p,x} \simeq \Omega_{p,z} \approx 0$ and maximum $\Omega_{p,y} \approx 0.05$. During the whole interaction, $|\Omega_{s,y}| \gg |\Omega_{p,y}|$ with opposite precession directions [see Figs. 3(b) and 3(c)]. The spin-polarization direction of the electron beam is quickly changed to the LSP state (opposite direction between spin and momentum) at the first precession peak in region I, where the net phase retardation amounts to about $1.2\pi/2$. Then $|\Omega_{s,y}|$ and $|\Omega_{p,y}|$ decrease to zero and do not vary much, along with $\Delta\Phi_s$ and $\Delta\Phi_p$, in region II. Subsequently, $|\Omega_{s,y}|$ and $|\Omega_{p,y}|$ in turn increase rapidly when the electron interacts with the front edge of the main peak pulse, and then gradually vanish with the pulse falling edge over a relatively long time in region III. Thus a final spin rotation angle $|\Delta\Phi_s| \simeq 7.94\pi/2$ and matched momentum rotation angle $|\Delta\Phi_p| \simeq 0.86\pi/2$ with opposite signs can be acquired with the employed parameters, giving rise to a net phase retardation of about $0.8\pi/2$. This clearly demonstrates that essential spin-polarization rotation (from TSP to LSP state) can be achieved with spin and momentum in opposite directions. In fact, due to the asymmetric field distribution of the half-cycle terahertz pulse, the local time-integrated normalized magnetic field is sufficiently large (~ 220), thus the electron momentum and spin dynamics are substantially asymmetric. In addition, our

numerical simulations demonstrate that spin manipulation of the electrons from TSP to LSP state, or vice versa, should satisfy the condition $|\Delta\Phi_s - \Delta\Phi_p| = (2n - 1)\pi/2$ [or $\gamma \simeq 2.96 + (2n - 1) \times 3.83$, for given parameters], where n is a positive integer.

B. Particle beam in a frequency-chirped laser pulse

As demonstrated above, the polarization manipulation for particle beams mainly depends on the temporal asymmetry of the laser field, when the opposite spin rotations of the particle in the positive and negative half-cycles of the laser field do not compensate each other, resulting in the net spin rotation during the whole interaction. Thus, besides the subcycle terahertz pulse, a moderately linearly chirped Gaussian laser pulse could be another candidate as an all-optical spin rotator, since its temporal symmetry can be destroyed by the negative chirp effect [79,80]. In the simulations, the spatial distribution of the electromagnetic field takes into account up to $(w_0/z_r)^5$ order of the nonparaxial solution, where z_r is the Rayleigh length [81,82]. At sufficiently large b , with the instantaneous frequency slowing down, the pulse local carrier structure is changed with a few elongated optical cycles. In other words, obvious asymmetry arises in the laser field, even forming a quasi-static-positive region [80]. Such a chirped laser pulse could in principle be produced by frequency filter technique and adding low-amplitude negative wings or prepulses via introducing higher-order dispersive [83] or maybe the interaction with a relativistic ionization plasma [84,85].

Likewise, for the situation of a proton beam interacting with such a linearly chirped laser pulse, the proton spins oscillate initially only slightly, and the initial TSP state is well preserved, since the rotations in the positive and negative half-cycles of the laser field offset each other [in the range of $\eta/2\pi \lesssim 137$ in Figs. 4(a)–4(c)]. Due to the negative chirp effect, this is followed by the interaction with a quasistatic positive region of the laser pulse, resulting in the proton spin polarization rotated to the LSP state and tuned in a nearly single elongated cycle during the range of $137 \lesssim \eta/2\pi \lesssim 147$. Finally, the protons interact with the rear part of the laser pulse in the range of $\eta/2\pi \gtrsim 147$, and its spin oscillations become weaker and weaker and eventually die down. The final average polarization is $\bar{S}_z \simeq 98\%$, symmetrically distributed with respect to θ_y , and the compressed divergence in θ_x is less than 3° [see Fig. 4(d)]. Meanwhile, a remarkable acceleration for the proton beam is also achieved with an average energy gain of about 120 MeV and an energy spread $< 10\%$. These results may be optimized further by moderately increasing the laser focal radius, allowing the protons to experience a quasi-uniform laser field. For heavier charged particles like a triton, the spin rotation and energy gain are moderately reduced compared with those of a proton, because the spin manipulation efficiency mainly depends on the charge-to-mass ratio and g factor of the particle (see Fig. 4, blue-dashed curves). While, for much lighter leptons such as electrons and positrons (with smaller g factors, too), it is vice versa (see Fig. 4, red-dashed curves), and consequently a much weaker laser pulse can satisfy the requirements. For instance, interacting with a

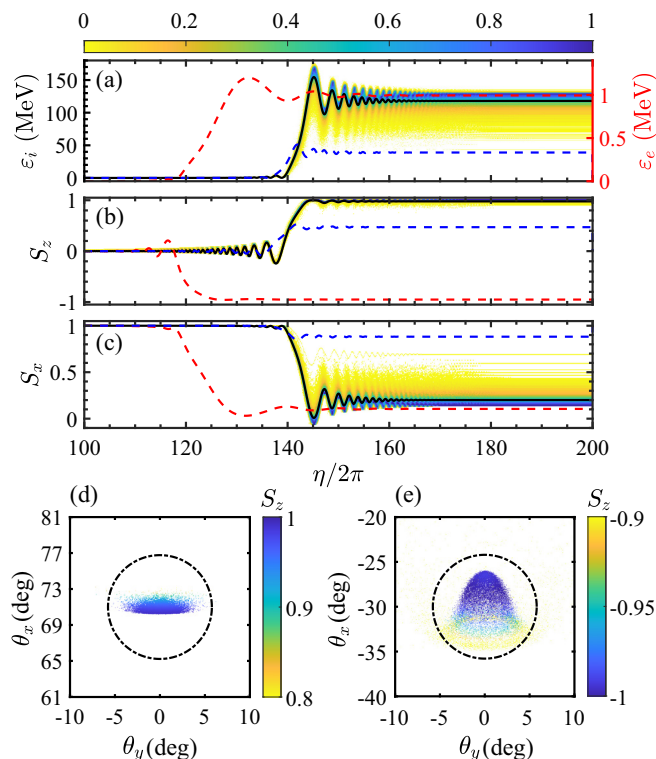


FIG. 4. (a)–(c) Variations of $dN/d\epsilon_i$, dN/dS_z and dN/dS_x of the proton beam (color) with respect to η , respectively, and the black curves show the corresponding average values. N is the particle number. The blue and red-dashed curves show the average values for the cases of interacting with a tritium and electron beam, respectively. For electrons, the initial energy of $\epsilon_0 = 0.1$ MeV. (d), (e) Angle-resolved distributions of S_z vs the transverse deflection angles θ_x and θ_y for the proton and electron beams, respectively. The black-dashed circles denote the corresponding beam initial profile sizes. Simulation parameters are given in the text.

tens-of-GW laser of $a_0 = 0.2$, the electron beam can achieve a final polarization of $\bar{S}_z \simeq -0.95$, with a bell-shaped angular distribution [see Fig. 4(e)]. Such a highly LSP low-divergence MeV electron beam or hundred-MeV proton beam can be employed as the polarized injection source for high-energy accelerators [70], to map electromagnetic fields structure in plasma [86], study polarized nuclear fusion [87], and search for new physics by investigating CP or T symmetry [8,88] (e.g., null high-precision tests of T violation by polarized proton-deuteron scattering at an energy of 135 MeV [89]).

The spin manipulation mechanism in this case is also analyzed in Fig. 5. During interaction with the front region of the laser field, $|\Omega_p| \gg |\Omega_s|$ ($\Omega_{p,x} \simeq \Omega_{p,z} \approx 0$ and $\Omega_{p,y} \approx 0.5$, $\Omega_{s,x} \simeq \Omega_{s,z} \approx 0$ and $\Omega_{s,y} \approx 0.064$) with opposite precession directions and the phase of $\Omega_{p,y}$ is ahead of that of $\Omega_{s,y}$ by π [see Figs. 5(b) and 5(c) in region I]. This clearly demonstrates that the spin-polarization direction of the proton beam is unchanged during interaction with region I (as well as region III) of the laser pulse, where the spin and momentum precession do not result in a net change in $\Delta\Phi_s$ and $\Delta\Phi_p$

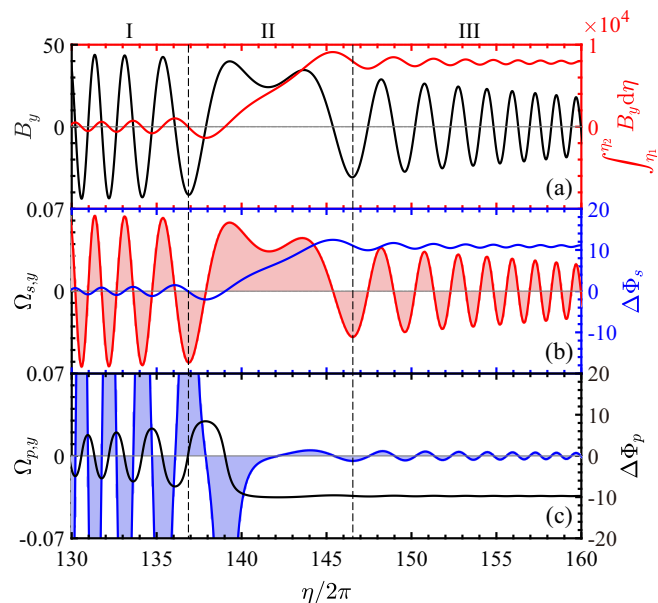


FIG. 5. (a) Evolutions of the normalized magnetic field B_y sensed by the proton (black) and its local time-integrated profile (red). (b) Spin precession frequency $\Omega_{s,y}$ (red) and $\Delta\Phi_s$ (blue) vs η . (c) Momentum angular frequency $\Omega_{p,y}$ (blue) and $\Delta\Phi_p$ (black) vs η . Other simulation parameters are the same as those in Fig. 4.

simultaneously. Tuning the laser field by an optimal linear negative chirp $b = -0.00539$, the formed intense quasistatic positive region (II) makes the proton momentum and spin rotation asymmetrical in the positive and negative half-cycles. The phase retardation $|\Delta\Phi_s - \Delta\Phi_p|$ decreases rapidly and then varies slightly over a relatively long time. Thus a comparable match of $|\Delta\Phi_s| \simeq 6.83\pi/2$ and $|\Delta\Phi_p| \simeq 6.19\pi/2$ of opposite signs can be acquired with the employed parameters, giving rise to a net phase retardation of about $\pi/2$ [see Figs. 5(b) and 5(c)]. Subsequently, sufficient spin-polarization rotation (from TSP to LSP state) can be achieved.

Regarding experimental feasibility, the impact of other laser and particle beam parameters on the efficiency of the spin rotation is investigated in Figs. 6 and 7. In the case of a subcycle terahertz pulse, the optimal LSP state is obtained for $\tau_0 = T_0/2$, which corresponds to $\varphi_0 = 0, \pm\pi$. The results stay stable within the adjustable range of $\tau_0 \pm 5\%$ ($\varphi_0 \pm 9.3\%$) for the parameters employed [see Figs. 6(a) and 6(b)]. The adjustable precision, $\delta S_z/S_z \sim 2.38\%$, is estimated using feasible a_0 and τ_0 parameter values which may result in fluctuations of about 0.01 [76,78]. Viewed as functions of the chirp parameter b , the final S_z and kinetic energy gain ε_p of the proton beam in the case of chirped laser exhibit local fluctuations of the order of 10^{-3} , with the optimal rotation occurring, for an optimal ε_p , for $b \approx -0.00539$ [see Fig. 6(c)] and $\varphi_0 = 0, \pm\pi$ [see Fig. 6(d)]. The corresponding adjustable precision of $\delta S_z/S_z \sim 0.27\%$ is higher for the generally feasible b and a_0 parameter values. Also, \bar{S}_z increases exponentially with a_0 and decreases with τ_0 , while \bar{S}_x follows an opposite trend [see Figs. 6(e) and 6(f)]. The final average energy gain, $\bar{\varepsilon}_p$, increases almost linearly

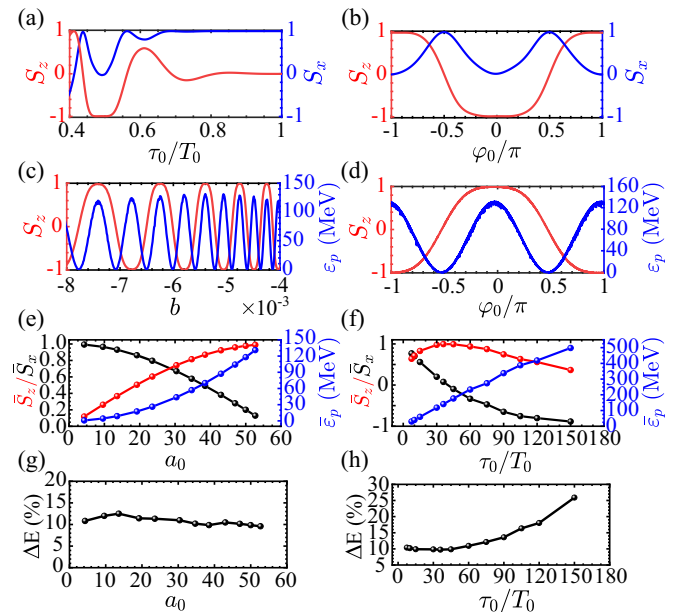


FIG. 6. (a), (b) Final S_z and S_x of the electron beam vs τ_0 and the carrier-envelope phase (CEP) φ_0 of the terahertz pulse, respectively. (c), (d) Final S_z , ε_p and (e), (f) average \bar{S}_z (red), \bar{S}_x (black), and $\bar{\varepsilon}_p$ of the proton beam vs b , φ_0 , a_0 , and τ_0 of the chirped laser pulse, respectively. (g), (h) The corresponding energy spread ΔE of the proton beam with the pulse a_0 and τ_0 . Other parameters are the same as those in Figs. 2 and 4.

with a_0 and τ_0 , while the energy spread nearly remains less than 10% with a_0 at shorter pulse duration [see Figs. 6(g) and 6(h)].

In addition, the spin rotation effect is optimal for a proton beam with a low initial kinetic energy of $\varepsilon_p \lesssim 50$ MeV [see Fig. 7(a)]. The final \bar{S}_z decreases almost exponentially with initial $S_z < 0$ and linearly with initial $S_z > 0$, while the final \bar{S}_x follows an opposite trend as well [see Fig. 7(b)]. Finally, our method is widely effective for temporally asymmetrical laser pulses, also including the case of laser pulses accompanied by additional intense low-frequency magnetic fields [90,91]; however, it is not applicable for scenarios that are spatially asymmetrical (e.g., bichromatic; see Fig. 8 in the Appendix).

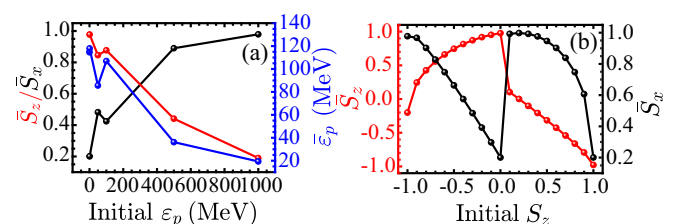


FIG. 7. (a), (b) Final \bar{S}_x (black), \bar{S}_z (red), and kinetic energy gain $\bar{\varepsilon}_p$ (blue) vs the initial kinetic energy ε_p and the initial spin S_z of the proton beam, respectively. Other parameters are the same as those in Fig. 4.

IV. CONCLUSIONS

An all-optical ultrafast spin rotation method has been put forward to precisely manipulate the polarization of relativistic charged particle beams using a moderate temporally asymmetrical laser pulse. This method is feasible with currently available laser facilities and would provide a technique for carrying out polarized beam experiments and high-precision spin-dependent measurements in laser-plasma, laser-nuclear, and high-energy particle physics.

ACKNOWLEDGMENTS

This work has been supported by the National Natural Science Foundation of China (Grants No. U2030104, No. U2267204, No. 12105218, No. 12022506, No. 11975174, and No. 11874295), National Key Research and Development Program of China (Grant No. 2019YFA0404900), Chinese Science Challenge Project (Grant No. TZ2016005), the China Postdoctoral Science Foundation (Grant No. 2020M673367), and Science and Technology on Plasma Physics Laboratory (Grant No. J202108010). Y.I.S. is supported by an American University of Sharjah Faculty Research Grant (Grant No. FRG21).

APPENDIX

The spin rotation processes of the proton beam in the spatially asymmetric (bichromatic) laser pulses are shown in Fig. 8, respectively. For this case, the proton spins oscillate slightly in the laser field and no net spin rotation is obtained, i.e., the initial TSP state is well preserved and the spin rotation does not occur.

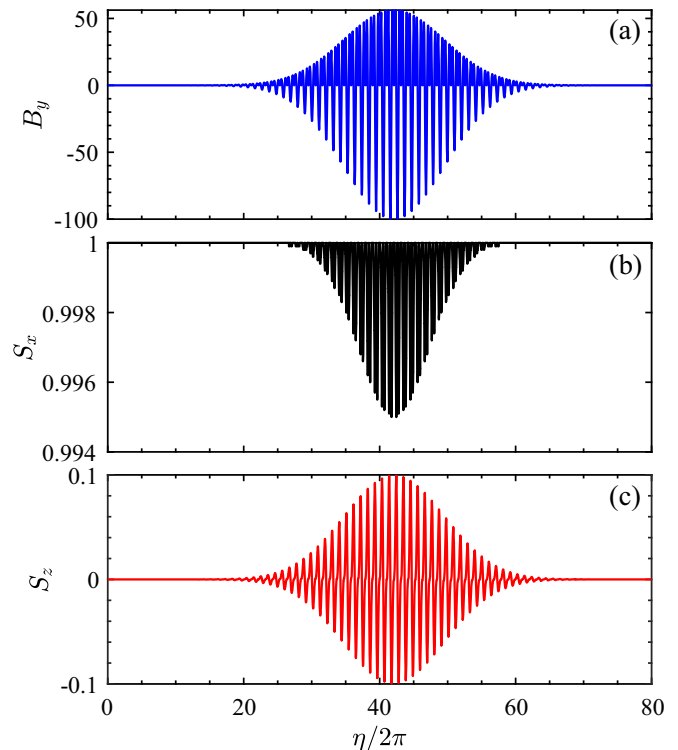


FIG. 8. (a)–(c) Evolutions of B_y sensed by the proton, S_x and S_z , respectively, in the bichromatic laser field. The electromagnetic components of the bichromatic laser field are as follows: $B_y \simeq E_x = [a_0 \cos(\varphi_0 + \eta) + a_0 \cos(\varphi_0 + 2\eta + \phi)] \exp[-(\eta - 4\tau_0/T_0)^2 / (\tau_0/T_0)^2]$ and other components are vanishing, where $\phi = \pi$ is the relative phase, $\varphi_0 = 0$ the CEP phase, $a_0 = 50$, and $\tau_0 = 10T_0$. Other parameters are the same as those in Fig. 4.

- [1] S. D. Bass, The spin structure of the proton, *Rev. Mod. Phys.* **77**, 1257 (2005).
- [2] M. Burkardt, C. A. Miller, and W.-D. Nowak, Spin-polarized high-energy scattering of charged leptons on nucleons, *Rep. Prog. Phys.* **73**, 016201 (2010).
- [3] C. A. Aidala, S. D. Bass, D. Hasch, and G. K. Mallot, The spin structure of the nucleon, *Rev. Mod. Phys.* **85**, 655 (2013).
- [4] Y.-B. Yang *et al.* (χ QCD Collaboration), Glue Spin and Helicity in the Proton from Lattice QCD, *Phys. Rev. Lett.* **118**, 102001 (2017).
- [5] A. Accardi, J. L. Albacete, M. Anselmino, N. Armesto, E. C. Aschenauer, A. Bacchetta, D. Boer, W. K. Brooks, T. Burton, N.-B. Chang, W.-T. Deng, A. Deshpande, M. Diehl, A. Dumitru, R. Dupré, R. Ent, S. Fazio, H. Gao, V. Guzey, H. Hakobyan *et al.*, Electron-ion collider: The next QCD frontier, *Eur. Phys. J. A* **52**, 268 (2016).
- [6] N. Severijns, M. Beck, and O. Naviliat-Cuncic, Tests of the standard electroweak model in nuclear beta decay, *Rev. Mod. Phys.* **78**, 991 (2006).
- [7] M. T. Gericke *et al.* (n^3 He Collaboration), First Precision Measurement of the Parity Violating Asymmetry in Cold Neutron Capture on ^3He , *Phys. Rev. Lett.* **125**, 131803 (2020).
- [8] G. Moortgat-Pick, T. Abe, G. Alexander, B. Ananthanarayan, A. Babich, V. Bharadwaj, D. Barber, A. Bartl, A. Brachmann, S. Chen, J. Clarke, J. Clendenin, J. Dainton, K. Desch, M. Diehl, B. Dobos, T. Dorland, H. Dreiner, H. Eberl, J. Ellis *et al.*, Polarized positrons and electrons at the linear collider, *Phys. Rep.* **460**, 131 (2008).
- [9] E. C. Aschenauer, S. Fazio, J. H. Lee, H. Mäntysaari, B. S. Page, B. Schenke, T. Ullrich, R. Venugopalan, and P. Zurita, The electron-ion collider: Assessing the energy dependence of key measurements, *Rep. Prog. Phys.* **82**, 024301 (2019).
- [10] D. Androić *et al.* (Jefferson Lab Qweak Collaboration), Precision measurement of the weak charge of the proton, *Nature (London)* **557**, 207 (2018).
- [11] D. P. Anderle, V. Bertone, X. Cao, L. Chang, N. Chang, G. Chen, X. Chen, Z. Chen, Z. Cui, L. Dai, W. Deng, M. Ding, X. Feng, C. Gong, L. Gui, F.-K. Guo, C. Han, J. He, T.-J. Hou, H. Huang *et al.*, Electron-ion collider in China, *Front. Phys.* **16**, 64701 (2021).
- [12] L. Rosen, Polarized protons as nuclear probes, *Science* **157**, 1127 (1967).
- [13] J. Tojo, I. Alekseev, M. Bai, B. Bassalleck, G. Bunce, A. Deshpande, J. Doskow, S. Eilerts, D. E. Fields, Y. Goto, H. Huang, V. Hughes, K. Imai, M. Ishihara, V. Kanavets, K. Kurita, K. Kwiatkowski, B. Lewis, W. Lozowski, Y. Makdisi *et al.*, Measurement of Analyzing Power for Proton-Carbon Elastic Scattering in the Coulomb-Nuclear Interference Region with a 22-GeV/c Polarized Proton Beam, *Phys. Rev. Lett.* **89**, 052302 (2002).

- [14] C. E. Allgower *et al.* (E925 Collaboration), Measurement of analyzing powers of π^+ and π^- produced on a hydrogen and a carbon target with a 22-GeV/ c incident polarized proton beam, *Phys. Rev. D* **65**, 092008 (2002).
- [15] M. Temporal, V. Brandon, B. Canaud, J. Didelez, R. Fedosejevs, and R. Ramis, Ignition conditions for inertial confinement fusion targets with a nuclear spin-polarized DT fuel, *Nucl. Fusion* **52**, 103011 (2012).
- [16] G. Hupin, S. Quaglioni, and P. Navrátil, *Ab initio* predictions for polarized deuterium-tritium thermonuclear fusion, *Nat. Commun.* **10**, 351 (2008).
- [17] D. de Florian, R. Sassot, M. Stratmann, and W. Vogelsang, Evidence for Polarization of Gluons in the Proton, *Phys. Rev. Lett.* **113**, 012001 (2014).
- [18] C. Alexandrou, M. Constantinou, K. Hadjiyiannakou, K. Jansen, C. Kallidonis, G. Koutsou, A. V. Avilés-Casco, and C. Wiese, Nucleon Spin and Momentum Decomposition Using Lattice QCD Simulations, *Phys. Rev. Lett.* **119**, 142002 (2017).
- [19] L. Adamczyk *et al.* (STAR Collaboration), Measurement of Longitudinal Spin Asymmetries for Weak Boson Production in Polarized Proton-Proton Collisions at RHIC, *Phys. Rev. Lett.* **113**, 072301 (2014).
- [20] L. Adamczyk *et al.* (STAR Collaboration), Measurement of the Transverse Single-Spin Asymmetry in $p^\dagger + p \rightarrow W^\pm/Z^0$ at RHIC, *Phys. Rev. Lett.* **116**, 132301 (2016).
- [21] M. S. Abdallah *et al.* (STAR Collaboration), Longitudinal double-spin asymmetry for inclusive jet and dijet production in polarized proton collisions at $\sqrt{s} = 200$ GeV, *Phys. Rev. D* **103**, L091103 (2021).
- [22] C. Aidala *et al.* (PHENIX Collaboration), Cross section and transverse single-spin asymmetry of muons from open heavy-flavor decays in polarized $p + p$ collisions at $\sqrt{s} = 200$ GeV, *Phys. Rev. D* **95**, 112001 (2017).
- [23] S. S. Adler *et al.* (PHENIX Collaboration), Double Helicity Asymmetry in Inclusive Midrapidity π^0 Production for Polarized $p + p$ Collisions at $\sqrt{s} = 200$ GeV, *Phys. Rev. Lett.* **93**, 202002 (2004).
- [24] A. Zelenski, J. Alessi, B. Briscoe, G. Dutto, H. Huang, A. Kponou, S. Kokhanovski, V. Klenov, A. Lehrach, P. Levy, V. LoDestro, Y. Mori, M. Okamura, D. Raparia, J. Ritter, T. Takeuchi, G. Wight, and V. Zoubets, Optically pumped polarized H^- ion source for RHIC spin physics, *Rev. Sci. Instrum.* **73**, 888 (2002).
- [25] G. H. Hoffstaetter, *High-Energy Polarized Proton Beams: A Modern View* (Springer-Verlag, New York, 2006), Vol. 218.
- [26] C. K. Sinclair, P. A. Adderley, B. M. Dunham, J. C. Hansknecht, P. Hartmann, M. Poelker, J. S. Price, P. M. Rutt, W. J. Schneider, and M. Steigerwald, Development of a high average current polarized electron source with long cathode operational lifetime, *Phys. Rev. ST Accel. Beams* **10**, 023501 (2007).
- [27] A. A. Sokolov and I. M. Ternov, Synchrotron radiation, *Sov. Phys. J.* **10**, 39 (1967).
- [28] D. Barber, M. Böge, H.-D. Bremer, R. Brinkmann, W. Brückner, M. Düren, E. Gianfelice-Wendt, C. Großhauser, H. Kaiser, R. Klanner, M. Lomperski, G. Meyer, N. Meyners, P. Oelwein, G. Ripken, K. Rith, G. Schmidt, E. Steffens, W. Wander, W. Wümpelmann *et al.*, The first achievement of longitudinal spin polarization in a high energy electron storage ring, *Phys. Lett. B* **343**, 436 (1995).
- [29] Y. N. Filatov, A. M. Kondratenko, M. A. Kondratenko, Y. S. Derbenev, and V. S. Morozov, Transparent Spin Method for Spin Control of Hadron Beams in Colliders, *Phys. Rev. Lett.* **124**, 194801 (2020).
- [30] S. Y. Lee, *Spin Dynamics and Snakes in Synchrotrons* (World Scientific, Singapore, 1997).
- [31] H. Huang, J. Kewisch, C. Liu, A. Marusic, W. Meng, F. Méot, P. Oddo, V. Ptitsyn, V. Ranjbar, and T. Roser, High Spin-Flip Efficiency at 255 GeV for Polarized Protons in a Ring With Two Full Siberian Snakes, *Phys. Rev. Lett.* **120**, 264804 (2018).
- [32] S. Y. Lee and S. Tepikian, Resonance Due to a Local Spin Rotator in High-Energy Accelerators, *Phys. Rev. Lett.* **56**, 1635 (1986).
- [33] C. N. Danson, C. Haefner, J. Bromage, T. Butcher, J. Chanteloup, E. A. Chowdhury, A. Galvanauskas, L. A. Gizzi, J. Hein, D. I. Hillier, N. W. Hopps, Y. Kato, E. A. Khazanov, R. Kodama, G. Korn, R. Li, Y. Li, J. Limpert, J. Ma, C. H. Nam *et al.*, Petawatt and exawatt class lasers worldwide, *High Power Laser Sci. Eng.* **7**, e54 (2019).
- [34] J. W. Yoon, C. Jeon, J. Shin, S. K. Lee, H. W. Lee, I. W. Choi, H. T. Kim, J. H. Sung, and C. H. Nam, Achieving the laser intensity of 5.5×10^{22} W/cm² with a wavefront-corrected multi-PW laser, *Opt. Express* **27**, 20412 (2019).
- [35] J. W. Yoon, Y. G. Kim, I. W. Choi, J. H. Sung, H. W. Lee, S. K. Lee, and C. H. Nam, Realization of laser intensity over 10^{23} W/cm², *Optica* **8**, 630 (2021).
- [36] A. Higginson, R. J. Gray, M. King, R. J. Dance, S. Williamson, N. Butler, R. Wilson, R. Capdessus, C. Armstrong, and J. S. Green, Near-100 MeV protons via a laser-driven transparency-enhanced hybrid acceleration scheme, *Nat. Commun.* **9**, 724 (2018).
- [37] A. McIlvenny, D. Doria, L. Romagnani, H. Ahmed, N. Booth, E. J. Ditter, O. C. Ettlinger, G. S. Hicks, P. Martin, G. G. Scott, S. D. R. Williamson, A. Macchi, P. McKenna, Z. Najmudin, D. Neely, S. Kar, and M. Borghesi, Selective Ion Acceleration by Intense Radiation Pressure, *Phys. Rev. Lett.* **127**, 194801 (2021).
- [38] J. Ren, Z. Deng, W. Qi, B. Chen, B. Ma, X. Wang, S. Ying, J. Feng, W. Liu, Z. Xu, D. H. H. Hoffmann, S. Wang, Q. Fan, B. Cui, S. He, Z. Cao, Z. Zhao, L. Cao, Y. Gu, S. Zhu *et al.*, Observation of a high degree of stopping for laser-accelerated intense proton beams in dense ionized matter, *Nat. Commun.* **11**, 5157 (2020).
- [39] A. J. Gonsalves, K. Nakamura, J. Daniels, C. Benedetti, C. Pieronek, T. C. H. de Raadt, S. Steinke, J. H. Bin, S. S. Bulanov, J. van Tilborg, C. G. R. Geddes, C. B. Schroeder, C. Tóth, E. Esarey, K. Swanson, L. Fan-Chiang, G. Bagdasarov, N. Bobrova, V. Gasilov, G. Korn *et al.*, Petawatt Laser Guiding and Electron Beam Acceleration to 8 GeV in a Laser-Heated Capillary Discharge Waveguide, *Phys. Rev. Lett.* **122**, 084801 (2019).
- [40] D. Del Sorbo, D. Seipt, T. G. Blackburn, A. G. R. Thomas, C. D. Murphy, J. G. Kirk, and C. P. Ridgers, Spin polarization of electrons by ultraintense lasers, *Phys. Rev. A* **96**, 043407 (2017).
- [41] D. D. Sorbo, D. Seipt, A. G. R. Thomas, and C. P. Ridgers, Electron spin polarization in realistic trajectories around the magnetic node of two counter-propagating, circularly polarized, ultra-intense lasers, *Plasma Phys. Controlled Fusion* **60**, 064003 (2018).

- [42] D. Seipt, D. Del Sorbo, C. P. Ridgers, and A. G. R. Thomas, Theory of radiative electron polarization in strong laser fields, *Phys. Rev. A* **98**, 023417 (2018).
- [43] Y.-F. Li, R. Shaisultanov, K. Z. Hatsagortsyan, F. Wan, C. H. Keitel, and J.-X. Li, Ultrarelativistic Electron-Beam Polarization in Single-Shot Interaction with an Ultraintense Laser Pulse, *Phys. Rev. Lett.* **122**, 154801 (2019).
- [44] F. Wan, R. Shaisultanov, Y.-F. Li, K. Z. Hatsagortsyan, C. H. Keitel, and J.-X. Li, Ultrarelativistic polarized positron jets via collision of electron and ultraintense laser beams, *Phys. Lett. B* **800**, 135120 (2020).
- [45] D. Seipt, D. Del Sorbo, C. P. Ridgers, and A. G. R. Thomas, Ultrafast polarization of an electron beam in an intense bichromatic laser field, *Phys. Rev. A* **100**, 061402(R) (2019).
- [46] H.-H. Song, W.-M. Wang, J.-X. Li, Y.-F. Li, and Y.-T. Li, Spin-polarization effects of an ultrarelativistic electron beam in an ultraintense two-color laser pulse, *Phys. Rev. A* **100**, 033407 (2019).
- [47] Y.-Y. Chen, P.-L. He, R. Shaisultanov, K. Z. Hatsagortsyan, and C. H. Keitel, Polarized Positron Beams via Intense Two-Color Laser Pulses, *Phys. Rev. Lett.* **123**, 174801 (2019).
- [48] W.-Y. Liu, K. Xue, F. Wan, M. Chen, J.-X. Li, F. Liu, S.-M. Weng, Z.-M. Sheng, and J. Zhang, Trapping and acceleration of spin-polarized positrons from γ photon splitting in wakefields, *Phys. Rev. Res.* **4**, L022028 (2022).
- [49] Q. Zhao, L. Tang, F. Wan, B.-C. Liu, R.-Y. Liu, R.-Z. Yang, J.-Q. Yu, X.-G. Ren, Z.-F. Xu, Y.-T. Zhao, Y.-S. Huang, and J.-X. Li, Signatures of linear Breit-Wheeler pair production in polarized $\gamma\gamma$ collisions, *Phys. Rev. D* **105**, L071902 (2022).
- [50] Y.-F. Li, Y.-Y. Chen, W.-M. Wang, and H.-S. Hu, Production of Highly Polarized Positron Beams via Helicity Transfer from Polarized Electrons in a Strong Laser Field, *Phys. Rev. Lett.* **125**, 044802 (2020).
- [51] K. Xue, R.-T. Guo, F. Wan, R. Shaisultanov, Y.-Y. Chen, Z.-F. Xu, X.-G. Ren, K. Z. Hatsagortsyan, C. H. Keitel, and J.-X. Li, Generation of arbitrarily polarized GeV lepton beams via nonlinear Breit-Wheeler process, *Fundamental Res.* **2**, 539 (2022).
- [52] K. Ta Phuoc, S. Corde, C. Thaury, V. Malka, A. Tafzi, J. P. Goddet, R. C. Shah, S. Sebban, and A. Rousse, All-optical Compton gamma-ray source, *Nat. Photonics* **6**, 308 (2012).
- [53] D. Abbott *et al.* (PEPPo Collaboration), Production of Highly Polarized Positrons Using Polarized Electrons at MeV Energies, *Phys. Rev. Lett.* **116**, 214801 (2016).
- [54] Z. Nie, F. Li, F. Morales, S. Patchkovskii, O. Smirnova, W. An, N. Nambu, D. Matteo, K. A. Marsh, F. Tsung, W. B. Mori, and C. Joshi, *In Situ* Generation of High-Energy Spin-Polarized Electrons in a Beam-Driven Plasma Wakefield Accelerator, *Phys. Rev. Lett.* **126**, 054801 (2021).
- [55] M. Wen, M. Tamburini, and C. H. Keitel, Polarized Laser-WakeField-Accelerated Kiloampere Electron Beams, *Phys. Rev. Lett.* **122**, 214801 (2019).
- [56] Y. Wu, L. Ji, X. Geng, J. Thomas, M. Büscher, A. Pukhov, A. Hützen, L. Zhang, B. Shen, and R. Li, Spin filter for polarized electron acceleration in plasma wakefields, *Phys. Rev. Appl.* **13**, 044064 (2020).
- [57] Z. Gong, Y. Shou, Y. Tang, and X. Yan, Energetic spin-polarized proton beams from two-stage coherent acceleration in laser-driven plasma, *Phys. Rev. E* **102**, 053212 (2020).
- [58] L. Jin, M. Wen, X. Zhang, A. Hützen, J. Thomas, M. Büscher, and B. Shen, Spin-polarized proton beam generation from gas-jet targets by intense laser pulses, *Phys. Rev. E* **102**, 011201(R) (2020).
- [59] X. F. Li, P. Gibbon, A. Hützen, M. Büscher, S. M. Weng, M. Chen, and Z. M. Sheng, Polarized proton acceleration in ultraintense laser interaction with near-critical-density plasmas, *Phys. Rev. E* **104**, 015216 (2021).
- [60] A. K. Spiliotis, M. Xygkis, M. E. Koutrakis, K. Tazes, G. K. Boulogiannis, C. S. Kannis, G. E. Katsoprinakis, D. Sofikitis, and T. P. Rakitzis, Ultrahigh-density spin-polarized hydrogen isotopes from the photodissociation of hydrogen halides: new applications for laser-ion acceleration, magnetometry, and polarized nuclear fusion, *Light: Sci. Appl.* **10**, 35 (2021).
- [61] D. Sofikitis, C. S. Kannis, G. K. Boulogiannis, and T. P. Rakitzis, Ultrahigh-Density Spin-Polarized H and D Observed via Magnetization Quantum Beats, *Phys. Rev. Lett.* **121**, 083001 (2018).
- [62] T. P. Rakitzis, P. C. Samartzis, R. L. Toomes, T. N. Kitsopoulos, A. Brown, G. G. Balint-Kurti, O. S. Vasyutinskii, and J. A. Beswick, Spin-polarized hydrogen atoms from molecular photodissociation, *Science* **300**, 1936 (2003).
- [63] V. I. Ritus, Quantum effects of the interaction of elementary particles with an intense electromagnetic field, *J. Sov. Laser Res.* **6**, 497 (1985).
- [64] V. N. Baier, V. M. Katkov, and V. M. Strakhovenko, *Electromagnetic Processes at High Energies in Oriented Single Crystals* (World Scientific, Singapore, 1998).
- [65] V. Baier and V. Katkov, Radiational polarization of electrons in inhomogeneous magnetic field, *Phys. Lett. A* **24**, 327 (1967).
- [66] M. W. Walser, D. J. Urbach, K. Z. Hatsagortsyan, S. X. Hu, and C. H. Keitel, Spin and radiation in intense laser fields, *Phys. Rev. A* **65**, 043410 (2002).
- [67] A. Di Piazza, C. Müller, K. Z. Hatsagortsyan, and C. H. Keitel, Extremely high-intensity laser interactions with fundamental quantum systems, *Rev. Mod. Phys.* **84**, 1177 (2012).
- [68] M. Wen, C. H. Keitel, and H. Bauke, Spin-one-half particles in strong electromagnetic fields: Spin effects and radiation reaction, *Phys. Rev. A* **95**, 042102 (2017).
- [69] A. Gonoskov, T. G. Blackburn, M. Marklund, and S. S. Bulanov, Charged particle motion and radiation in strong electromagnetic fields, *Rev. Mod. Phys.* **94**, 045001 (2022).
- [70] S. R. Mane, Y. M. Shatunov, and K. Yokoya, Spin-polarized charged particle beams in high-energy accelerators, *Rep. Prog. Phys.* **68**, 1997 (2005).
- [71] J. Thomas, A. Hützen, A. Lehrach, A. Pukhov, L. Ji, Y. Wu, X. Geng, and M. Büscher, Scaling laws for the depolarization time of relativistic particle beams in strong fields, *Phys. Rev. Accel. Beams* **23**, 064401 (2020).
- [72] L. H. Thomas, The motion of the spinning electron, *Nature (London)* **117**, 514 (1926).
- [73] L. H. Thomas, I. The kinematics of an electron with an axis, *London, Edinburgh Dublin Philos. Mag. J. Sci.* **3**, 1 (1927).
- [74] V. Bargmann, L. Michel, and V. L. Telegdi, Precession of the Polarization of Particles Moving in a Homogeneous Electromagnetic Field, *Phys. Rev. Lett.* **2**, 435 (1959).
- [75] See details of the g factor for particles of electron, proton, deuterium, and tritium ions on https://physics.nist.gov/cgi-bin/cuu/Results?search_for=g+factor.

- [76] G.-Q. Liao, H. Liu, G. G. Scott, Y.-H. Zhang, B.-J. Zhu, Z. Zhang, Y.-T. Li, C. Armstrong, E. Zemaityte, P. Bradford, D. R. Rusby, D. Neely, P. G. Huggard, P. McKenna, C. M. Brenner, N. C. Woolsey, W.-M. Wang, Z.-M. Sheng, and J. Zhang, Towards Terawatt-Scale Spectrally Tunable Terahertz Pulses via Relativistic Laser-Foil Interactions, *Phys. Rev. X* **10**, 031062 (2020).
- [77] G.-Q. Liao and Y.-T. Li, Review of intense terahertz radiation from relativistic laser-produced plasmas, *IEEE Trans. Plasma Sci.* **47**, 3002 (2019).
- [78] S. Herzer, A. Woldegeorgis, J. Polz, A. Reinhard, M. Almassarani, B. Beleites, F. Ronneberger, R. Grosse, G. G. Paulus, U. Hübner, T. May, and A. Gopal, An investigation on THz yield from laser-produced solid density plasmas at relativistic laser intensities, *New J. Phys.* **20**, 063019 (2018).
- [79] B. J. Galow, Y. I. Salamin, T. V. Liseykina, Z. Harman, and C. H. Keitel, Dense Monoenergetic Proton Beams from Chirped Laser-Plasma Interaction, *Phys. Rev. Lett.* **107**, 185002 (2011).
- [80] Y. I. Salamin, J.-X. Li, B. J. Galow, Z. Harman, and C. H. Keitel, Laser acceleration of proton bunches by petawatt chirped linearly polarized laser pulses, *Phys. Rev. A* **85**, 063831 (2012).
- [81] Y. I. Salamin and C. H. Keitel, Electron Acceleration by a Tightly Focused Laser Beam, *Phys. Rev. Lett.* **88**, 095005 (2002).
- [82] Y. I. Salamin, G. R. Mocken, and C. H. Keitel, Electron scattering and acceleration by a tightly focused laser beam, *Phys. Rev. ST Accel. Beams* **5**, 101301 (2002).
- [83] P. Tournois, Acousto-optic programmable dispersive filter for adaptive compensation of group delay time dispersion in laser systems, *Opt. Commun.* **140**, 245 (1997).
- [84] J. M. Dias, C. Stenz, N. Lopes, X. Badiche, F. Blasco, A. Dos Santos, L. Oliveira e Silva, A. Mysyrowicz, A. Antonetti, and J. T. Mendonça, Experimental Evidence of Photon Acceleration of Ultrashort Laser Pulses in Relativistic Ionization Fronts, *Phys. Rev. Lett.* **78**, 4773 (1997).
- [85] D. F. Gordon, B. Hafizi, R. F. Hubbard, J. R. Peñano, P. Sprangle, and A. Ting, Asymmetric Self-Phase Modulation and Compression of Short Laser Pulses in Plasma Channels, *Phys. Rev. Lett.* **90**, 215001 (2003).
- [86] X. Y. An, M. Chen, J. X. Li, S. M. Weng, F. He, Z. M. Sheng, and J. Zhang, Mapping electromagnetic fields structure in plasma using a spin polarized electron beam, *Phys. Plasmas* **26**, 123106 (2019).
- [87] M. W. Ahmed and H. R. Weller, Nuclear spin-polarized proton and ^{11}B fuel for fusion reactors: Advantages of double polarization in the $^{11}\text{B}(p, \alpha)^8\text{Be}^*$ fusion reaction, *J. Fusion Energy* **33**, 103 (2014).
- [88] P. Lenisa, F. Rathmann, L. Barion, S. Barsov, S. Bertelli, V. Carassiti, G. Ciullo, M. Contalbrigo, A. C. Ramusino, S. Dymov, R. Engels, D. Eversheim, R. Gebel, K. Grigoryev, J. Haidenbauer, V. Hejny, H. Jagdfeld, A. Kacharava, I. Keshelashvili, A. Kononov *et al.*, Low-energy spin-physics experiments with polarized beams and targets at the cosy storage ring, *EPJ Tech. Instrum.* **6**, 2 (2019).
- [89] B. v. Przewoski, H. O. Meyer, J. T. Balewski, W. W. Daehnick, J. Doskow, W. Haerberli, R. Ibal, B. Lorentz, R. E. Pollock, P. V. Pancella, F. Rathmann, T. Rinckel, S. K. Saha, B. Schwartz, P. Thörngren-Engblom, A. Wellinghausen, T. J. Whitaker, and T. Wise, Analyzing powers and spin correlation coefficients for $p + d$ elastic scattering at 135 and 200 MeV, *Phys. Rev. C* **74**, 064003 (2006).
- [90] B. J. Zhu, Y. T. Li, D. W. Yuan, Y. F. Li, F. Li, G. Q. Liao, J. R. Zhao, J. Y. Zhong, F. B. Xue, S. K. He, W. W. Wang, F. Lu, F. Q. Zhang, L. Yang, K. N. Zhou, N. Xie, W. Hong, H. G. Wei, K. Zhang, B. Han *et al.*, Strong magnetic fields generated with a simple open-ended coil irradiated by high power laser pulses, *Appl. Phys. Lett.* **107**, 261903 (2015).
- [91] G. J. Williams, S. Patankar, D. A. Mariscal, V. T. Tikhonchuk, J. D. Bude, C. W. Carr, C. Goyon, M. A. Norton, B. B. Pollock, A. M. Rubenchik, G. F. Swadling, E. R. Tubman, and J. D. Moody, Laser intensity scaling of the magnetic field from a laser-driven coil target, *J. Appl. Phys.* **127**, 083302 (2020).